NANO LETTERS

Letter

pubs.acs.org/NanoLett

Electrically Controlled Nanoparticle Synthesis inside Nanopores

Kimberly Venta, Meni Wanunu,† and Marija Drndić*

Department of Physics and Astronomy, University of Pennsylvania, Philadelphia, Pennsylvania 19104, United States

Supporting Information

ABSTRACT: From their realization just over a decade ago, nanopores in silicon nitride membranes have allowed numerous transport-based single-molecule measurements. Here we report the use of these nanopores as subzeptoliter mixing volumes for the controlled synthesis of metal nanoparticles. Particle synthesis is controlled and monitored through an electric field applied across the nanopore membrane, which is positioned so as to separate electrolyte solutions of a metal precursor and a reducing agent. When the electric field drives reactive ions to the nanopore, a characteristic drop in the ion current is observed, indicating the formation of a nanoparticle inside the nanopore. While traditional chemical synthesis relies on temperature and timing to monitor particle growth, here we observe it in real time by monitoring electrical current. We describe the dynamics of gold particle formation in sub-10 nm diameter silicon nitride pores and the effects of salt concentration and additives on the particle's shape and size. The current versus time signal during particle formation in the nanopore is in excellent agreement with the Richards growth curve, indicating an access-limited growth mechanism.

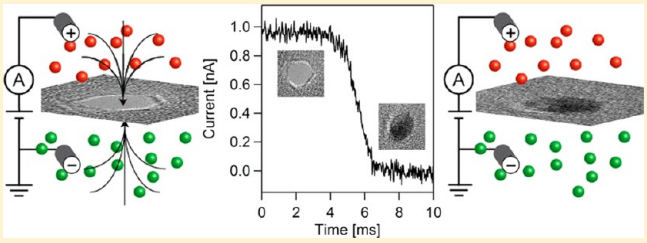

KEYWORDS: *Nanopores, nanoparticles, silicon nitride, synthesis, transmission electron microscopy, metallic nanostructures*

Methods for fabricating nanoparticles generally rely on either bottom-up approaches,[1−6] which are generally limited in the exact positioning of nanoparticles on a chip, or top-down approaches based on electron beam lithography,[7,8] which are limited in the smallest particle size that can be achieved. Confining chemical reactions by limiting reagent access is another approach to synthesizing nanostructures and has been used to make organic particles in solution,[9] high aspect ratio nanowires,[10] and electrofunctionalized micropores[11] as well as studies of precipitation-induced ion current fluctuations in nanopores[12] and related mathematical modeling.[13] Controllable synthesis could be useful for a range of applications including transport measurements, self-assembly, and catalysis. While solid-state nanopores have been mostly used for studies of electric-field-driven translocations of single molecules through the pores,[14−16] these pores are nanometer-size regions placed at desired locations on a solid-state chip and are thus unique candidates for studies of chemical reactions in confined volumes.

In this paper, we report the synthesis of sub-10 nm metal nanoparticles inside silicon nitride (SiN_x) nanopores placed at desired positions on a chip. The nanopores are predrilled with the condensed electron beam of a transmission electron microscope (TEM)[17,18] near thinned marker regions patterned on a silicon nitride membrane. These markers help us locate a single nanopore on a silicon nitride membrane. Gold particle synthesis is monitored in real time by measuring the ionic current; this current decreases to zero when the particle fills the nanopore. The resulting nanoparticles are then found in the TEM using the reference markers and imaged with atomic scale resolution (Figure 6). One advantage of this synthesis method over traditional chemical synthesis[19,20] is that we observe particle growth directly through these electrical measurements instead of relying on temperature and timing to estimate particle size.

We used nanopores with diameters ranging from 4 to 20 nm fabricated through silicon nitride (SiN_x) membranes. Figure 1a and b is TEM images of a single 6.5 nm diameter nanopore and a larger view showing four 200-nm-large prepatterned reference regions where SiN_x was etched. Figure 1c is a schematic diagram of the SiN_x membrane and supporting SiO_2/Si chip. We used low-stress (200−300 MPa), 25-nm-thick, amorphous silicon nitride (SiN_x) on top of 5 μm of SiO_2 grown on 500 μm thick n-type silicon. Four inch wafers produced many 5 × 5 mm^2 square chips each with a 50 × 50 μm^2 region in their center where the SiN_x membrane was freely suspended as previously described.[21,22] We patterned markers by thinning squares in the membrane (Figure 1b) using electron beam lithography followed by reactive ion etching.[23] Nanopores were drilled on a JEOL 2010F transmission electron microscope[17] set at 200 kV accelerating voltage.

The nanoparticle synthesis procedure inside the nanopore is illustrated in Figure 1d−f. To begin, the SiN_x membrane was placed in a measurement setup so that it divides two 100 μL polytetrafluoroethylene (PTFE) chambers (designated A and B) of salt solution, and a Ag/AgCl electrode was placed in each chamber (Figure 1d). Potassium chloride (KCl) with concentrations from 5 mM to 1 M was used as an electrolyte

Received: September 25, 2012
Revised: December 14, 2012

   dx.doi.org/10.1021/nl303576q | *Nano Lett.* XXXX, XXX, XXX−XXX

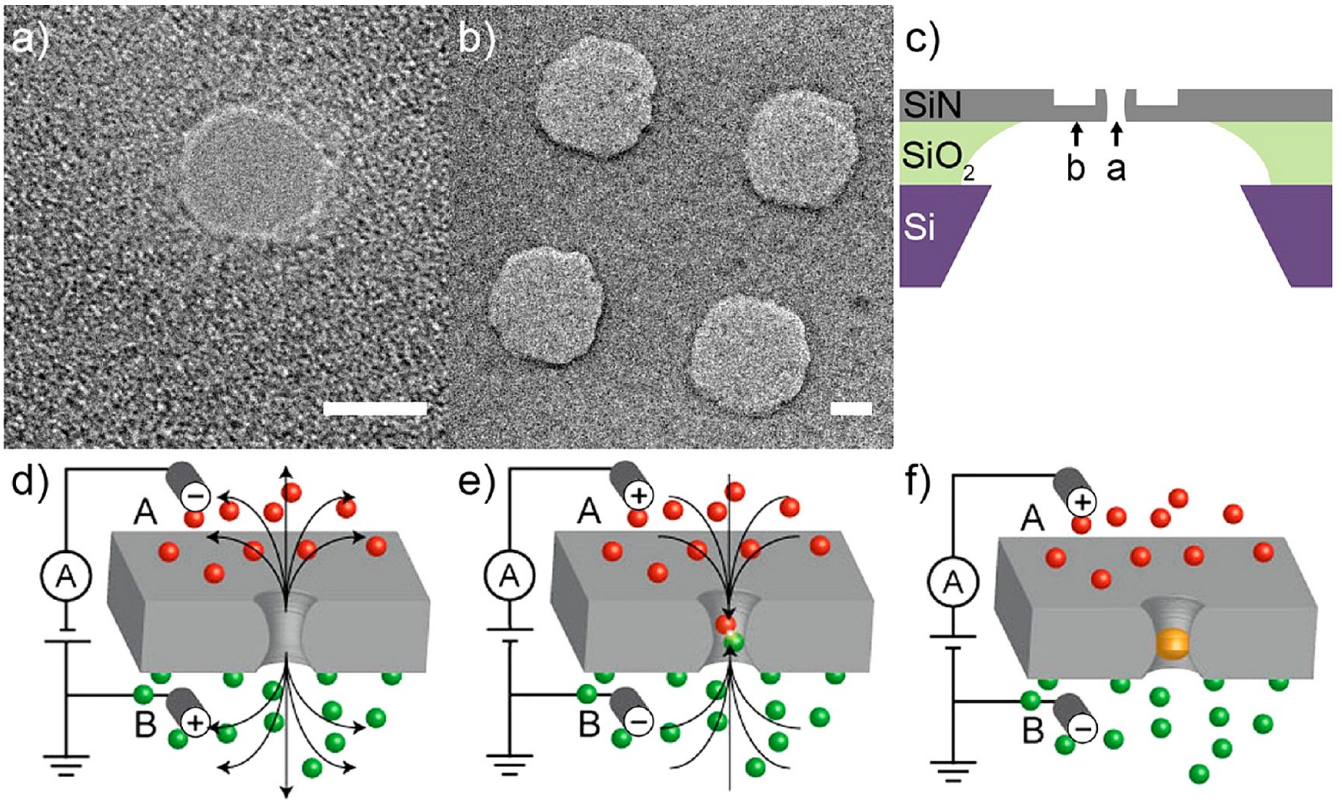

Figure 1. Electric-field-driven nanoparticle synthesis in a nanopore. (a) TEM image of a 6.5 nm diameter nanopore in a SiN_x membrane. The scale bar is 5 nm. (b) Zoomed out TEM image of a SiN_x membrane. Membrane is prepatterned and thinned to form 200 nm × 200 nm square regions (light gray) used as markers. The scale bar is 100 nm. (c) Schematic of the membrane and support structure (not to scale). (d–f) Schematics of the particle growth process: (d) a SiN_x membrane with a single nanometer-size pore separates two chambers, A and B, of electrolyte. For Au synthesis, negatively charged gold(III) chloride is injected in chamber B, and positively charged hydrazine is injected in chamber A. At first, a potential applied across the chambers prevents the solutions from reacting. (e) The reaction is triggered by reversing the sign of the voltage difference, which drives the reagents into the pore where they react. (f) As the reagents react, a gold nanoparticle forms in the pore and in the process stops further reaction by preventing the reagents from mixing.

for measuring current through the pore. Application of a voltage difference ΔV in the range of a few hundred mV provided an electric field through the pore, which was enough to drive measurable ion current (of the order of a few nA) across the nanopore. For Au particle synthesis, while keeping $\Delta V < 0$, we added 20 μL of a 5 mg/mL solution of $HAuCl_4$ (gold(III) chloride) to chamber B and exchanged the solution in chamber A with 0.1 mass percent hydrazine solution, giving final concentrations of 2.94 mM $HAuCl_4$ and 0.0312 mM hydrazine. We chose these concentrations after varying the gold chloride concentration to find the value that minimized the time to form a particle (see Figure S1). Due to the safety hazards associated with hydrazine and practical concerns, we did not increase the hydrazine concentration any further. $AuCl_4^-$ is negatively charged at neutral pH, and hydrazine is a strong reducing agent that has a positive charge at neutral pH ($pK_a = 7.99$).[24] Therefore, keeping $\Delta V < 0$ mutually prevents the mixing of both reagents in the pore, shown in Figure 1d. In some experiments, we mixed 3.1 mM gold chloride in water with 0.03 M α-lipoic acid in water in a 2:1 ratio. The α-lipoic acid and gold form a complex that was used in place of the gold chloride, in the same volumes. To trigger particle nucleation at a desired moment, the sign of ΔV was suddenly reversed to a positive value, and both hydrazine and gold(III) chloride ions were driven through the pore, where the following reaction takes place in the confined pore environment to form a gold particle (see Figure 1e):

$$5AuCl_4^- + 4N_2H_5 \leftrightarrow 5Au_{(s)} + 20HCl + 4N_2$$

The formation of gold in the pore is self-limiting; that is, when gold completely fills the pore, the reagents can no longer access each other, and the reaction stops (Figure 1f). Both stock solutions of reagents were dissolved in the same molarity of KCl as the experiment's electrolyte. All experiments were performed at room temperature. We reused pores for multiple experiments by soaking them in aqua regia for 10 min to remove the gold particle. We additionally performed control experiments in which only one chamber was filled with reagent; that is, either hydrazine was present but gold chloride was not, or gold chloride was present but hydrazine was not (see Figure S2 in the Supporting Information). In all cases, the conductance after the voltage polarity was switched remained nonzero and approximately equal to the initial conductance, indicating that the pore remained open and no particle formed.

Prior to particle synthesis, we first checked that the measured ionic conductance agreed with our expected values based on the salt concentration and pore size determined by TEM imaging or conductance measurements[25] from previous particle formation experiments. For example, for a nanopore with a diameter of 5 nm, SiN_x thickness of 25 nm, and 1 M KCl solution, we expect ion conductance to be in the range of 7–8

dx.doi.org/10.1021/nl303576q | Nano Lett. XXXX, XXX, XXX–XXX

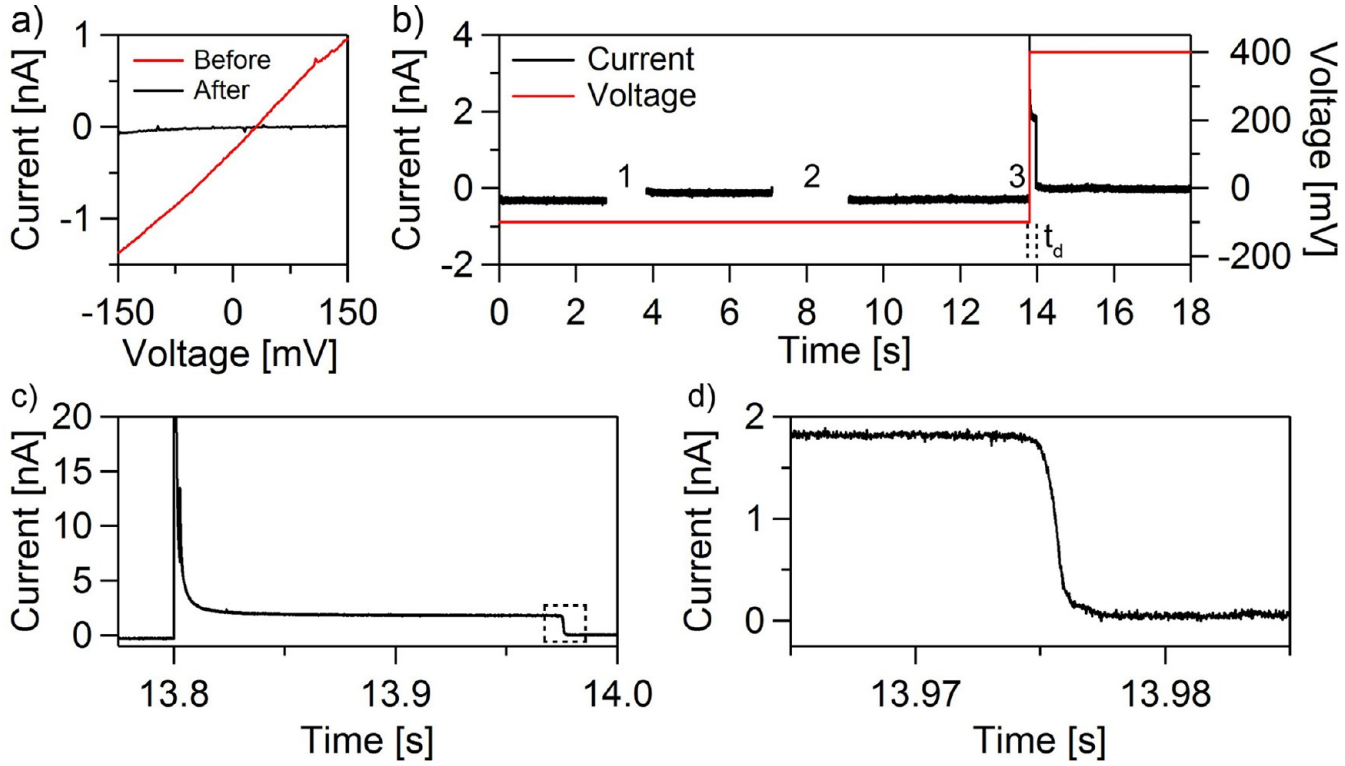

Figure 2. Current–voltage traces and current vs time traces during Au nanoparticle formation. (a) Current–voltage (I–V) traces for a nanopore before (red) and after (black) particle formation. For the empty pore trace, the ion current was measured in a solution of 5 mM KCl, without any hydrazine, gold chloride, or α-lipoic acid. (b) Current vs time trace and corresponding voltage vs time trace for a nanoparticle formation experiment on a 4.2 nm diameter pore in 5 mM KCl solution. (1) Hydrazine is injected to chamber A. The ion current shifts due to the chemical gradient that has formed. (2) Gold chloride is added to the chamber B, and the current again shifts. (3) Voltage polarity is reversed to electrically drive the reagents into the pore. The vertical dashed lines after (3) represent the time delay, t_d, before particle formation. The current then drops to zero when the particle forms. (c) Zoom-in of trace from voltage change to particle formation. The current spike is due to a capacitive response in our system. (d) Zoom-in from the dashed square in (c) highlighting the particle formation event. In over 80 experiments, these events display this characteristic sigmoid shape.

nS. A current–voltage (I–V) curve measured through a 15 nm diameter nanopore in 5 mM KCl solution is shown in Figure 2a (red line). The curve is linear because the conductance between electrodes is well-characterized by a model of resistors in series (see Figure S3 in the Supporting Information). The offset in the I–V trace we attribute to an offset in our electronics, which could be corrected by recalibrating the amplifier offset.

Figure 2b shows a voltage (ΔV) vs time trace and the corresponding ion current (I) vs time trace during one experiment to form a gold nanoparticle in a 4.2 nm diameter nanopore. In over 80 repeated experiments performed on over 10 nanopores, we find that the current trace during the growth of a particle follows a characteristic time trace described here. In this example, in the first ~2 s (Figure 2b) the chambers contained the 5 mM KCl solution with no precursors present, and $I = -0.31$ nA for $\Delta V = -100$ mV. At $t = 3$ s, while keeping ΔV constant and negative, hydrazine was injected to chamber A and I changed to −0.11 nA (labeled 1 in Figure 2b). The ion current shifted to a smaller value when hydrazine was added because the hydrazine created a chemical gradient that changed the ionic current flow through the pore. At $t = 8$ s, gold chloride was injected in chamber B, resulting in another current shift to −0.30 nA (labeled 2 in Figure 2b). The chemical reaction was triggered at $t = 13.8$ s by changing the polarity of ΔV from −100 mV to +400 mV (labeled 3 in Figure 2b). This sudden voltage change was accompanied by an initial current spike due to a capacitive response in our electrical circuit when voltage was changed, followed by particle formation which was indicated by a sudden current drop to zero. The current spike and particle formation are shown in Figure 2c. The capacitive response is slower than our sampling time of 20 μs, and an exponential fit to this response gives an equivalent RC time of ~0.4 ms. This is a well-known response that is seen when voltage is changed across a capacitor/resistive nanopore interface. Figure 2b and c is also present in control measurements, in which no particles were formed (see Figure S2 of the Supporting Information). The thick SiO_2 layer in our chips (Figure 1a) was specifically added to minimize capacitance thus reducing the RC time constant. The surface of the chips was also painted with a thick silicone elastomer to within ~1 mm of the membrane to further lower capacitance.

We performed current–voltage (I–V) traces before adding reagents (to prevent particle formation at positive ΔV) and after the experiment to verify that the particle has formed and fills the pore (Figure 2a). After changing the voltage, the conductance is within the noise level of zero and from a linear fit to the two lines is approximately 2% its original value, indicating the pore is now filled.

Figure 2d shows a magnified portion of the dashed box in the trace in Figure 2c that illustrates the ionic current readout of the particle formation process that follows this voltage change. In the left portion of the trace shown in Figure 2d ($t < 13.975$ s) the nanopore is completely open, as indicated by a constant current value ($I \sim 1.8$ nA at 400 mV). As gold nucleates, it

dx.doi.org/10.1021/nl303576q | Nano Lett. XXXX, XXX, XXX–XXX

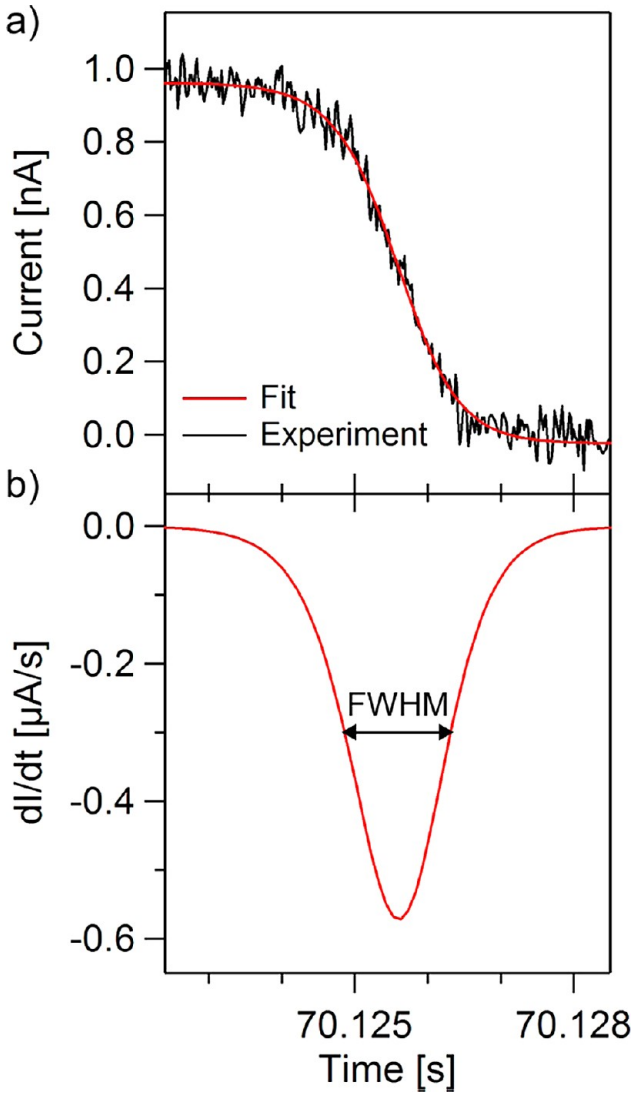

Figure 3. Richard's model fit of gold nanoparticle formation event inside a nanopore. (a) Fit to eq 3 of a particle formation event. The experiment was performed on a 4.2 nm diameter pore in 5 mM KCl. Voltage applied during formation was 300 mV. (b) Derivative of the fit, dI/dt, is shown in panel a. The full width at half max gives a quantitative measure of the duration of particle growth.

blocks ions from traversing the pore, and the ionic current decreases (13.975 s < t < 13.98 s, Figure 2d). Another event time trace is shown in Figure 3a (black trace) and the derivative of that trace's fit (Figure 3b). The trace in Figure 3a shows the same characteristics. Additionally, in Figure 3b, we plot the rate of current change dI/dt. This rate (and thus particle growth) greatly decreases at first as the nucleating cluster grows larger, until the particle is large enough to hinder incoming reagents from reacting, at which point particle growth slows down. When the gold nanoparticle completely fills the pore, ions and reagents can no longer traverse the pore, the ionic current stabilizes at zero, and the reaction stops (13.98 s < t, Figure 2b). Therefore, this reaction in the pore is self-limiting. Particles formed using this method are embedded in the membrane and confined to the nanopore volume, as confirmed by TEM imaging discussed below.

This sigmoid time dependence of the ion current during particle formation is very different from the sharp ion current

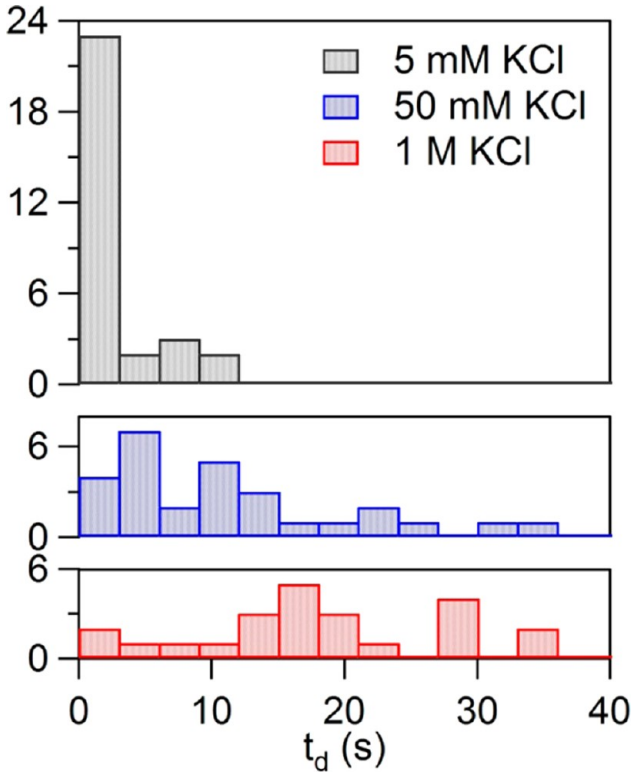

Figure 4. Histogram of the measured time delays, t_d; t_d is the time elapsed between the time when voltage polarity is reversed and the time when ion current goes to zero and the particle fills the pore completely. Data are shown for three different salt (KCl) concentrations: 5 mM (gray, top), 50 mM (blue, middle), and 1 M (red, bottom). The concentrations of reactants were held constant. From Poisson fits: for 1 M, t_d = 15 ± 1 s; for 50 mM t_d = 2.3 ± 0.5 s; and for 5 mM t_d = 0.8 ± 0.2 s.

decrease that is typically observed in biomolecular translocation as the biomolecule blocks the pore.[14−16,26] Below we present a model that explains our observations. Precipitation of cobalt hydrogen phosphate in a nanopore was previously modeled for conical polyethylene terephthalate nanopores of similar minimum radii,[13] but the different experimental conditions, materials, and pore geometry in the experiment presented here suggest the need for a different model. We find that the current signal observed here is well-described by the sigmoid Richards growth curve.[27] This curve was originally developed as a general model for biological growth, but it is applicable to our situation. The rate of particle growth is determined by the rate at which it accumulates gold from reagents, just as the rate of an organism's growth is determined by the rate at which it accumulates weight from food. The generalized equation is the solution to the differential equation

$$\frac{dW}{dt} = \eta W^m - \kappa W \quad (1)$$

where W is an organism's weight, t is time, η is the anabolic constant, κ is the catabolic constant, and m is an exponent determined by the biological situation. In the comparable case described here, W is the gold nanoparticle's radius, r, η is the particle growth constant, and κ is a constraint constant that represents the difficulty for reagents to meet in the narrow pore environment. Here we assume that the particle's growth rate depends on its cross-sectional area only. The force on the

dx.doi.org/10.1021/nl303576q | Nano Lett. XXXX, XXX, XXX−XXX

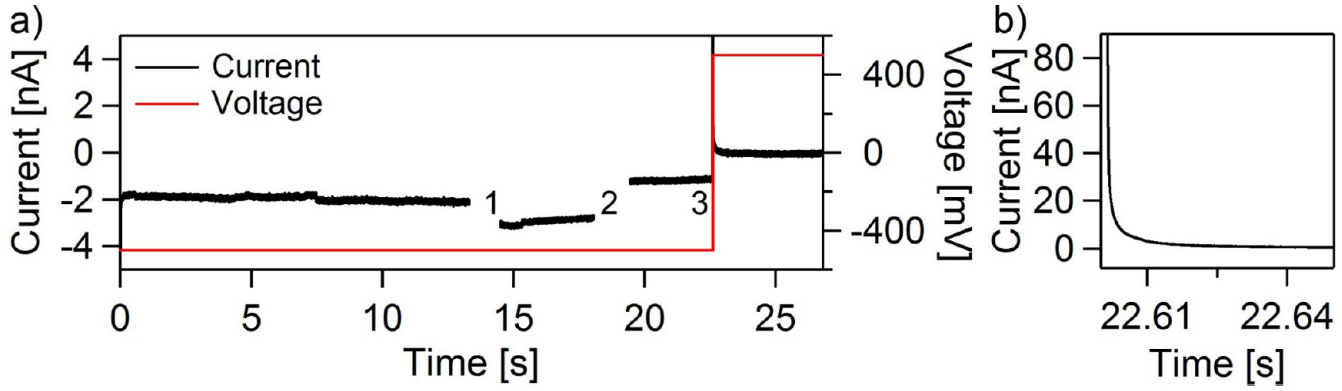

Figure 5. (a) Current vs time trace and corresponding voltage vs time trace for a nanoparticle formation experiment in the presence of α-lipoic acid. This experiment was performed on a 4.2 nm diameter pore in 50 mM KCl solution. (1), (2), and (3) represent the same experimental steps as in Figure 2b. (b) Zoom-in of (3) demonstrating that particle formation occurs faster than the limits of detection.

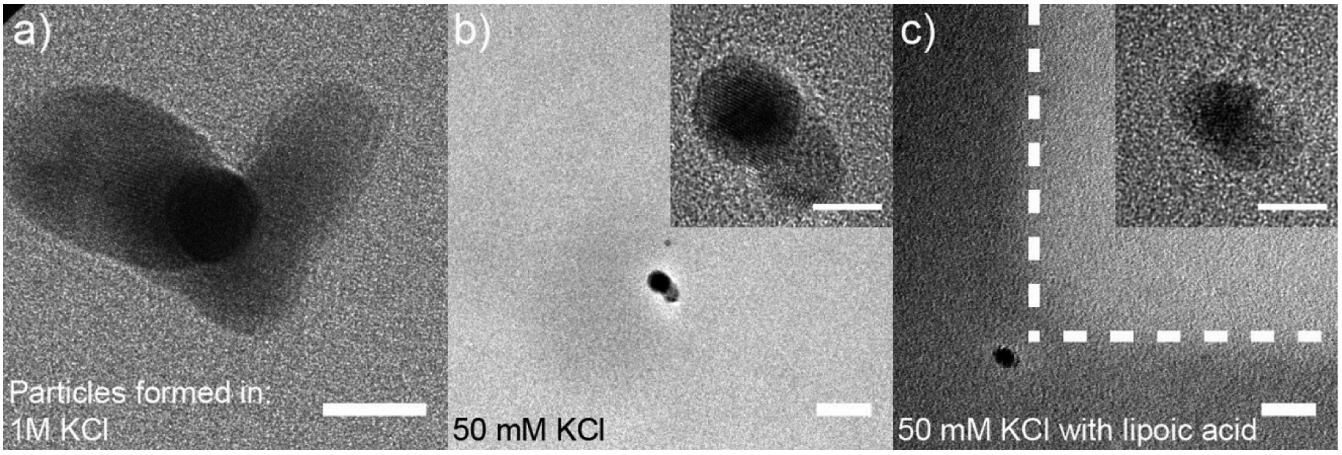

Figure 6. Transmission electron micrographs of particles synthesized in nanopores. Particles were formed using reagents in (a) 1 M KCl, (b) 50 mM KCl, and (c) 50 mM KCl with α-lipoic acid. Insets are zoomed in images of the particles. The scale bar is 10 nm in panel a, 20 nm in panels b and c, and 5 nm in the insets. For low salt concentrations ($\leq$50 mM), the chemical reaction is tightly confined to the nanopore, and gold is observed inside the pore only with no additional Au present in the vicinity, as seen in the larger views of the particle and surrounding SiN_x surface of panels b and c. The white dashed lines mark the boundary of the etched regions in SiN_x.

reagents drives them into the pore, where they encounter the particle's cross section, but there is no driving force pushing reagents to the sides of the particle parallel to the pore walls. Thus the value of the exponent m is 2. The constraint term κW is linear in radius because it depends on the length of the pore region that is constricted by the presence of the particle. In the case of $m = 2$, the solution to eq 1 is called the autocatalytic function:

$$r(t) = A(1 + be^{\kappa t})^{-1} \quad (2)$$

where $A = \kappa/\eta$, $b = 1 - \kappa/(\eta r_0)$, and r_0 is the radius of the nuclear particle. Since we measured ionic current instead of pore size and the ionic current through the pore is approximately proportional to the cross sectional area, we find the ionic current is given by

$$I(t) = C(\pi r_{\text{pore}}^2 - \pi r^2(t)) = I_0\left(1 - \frac{A_{\text{scaled}}}{(1 + be^{\kappa t})^2}\right) \quad (3)$$

where C is the proportionality constant, I_0 is the open pore current, and $A_{\text{scaled}} = A^2/r_{\text{pore}}^2$. Over 80 particle growth time traces were fit to this equation. A fit to the current vs time data using this model is shown in Figure 3a. From Gaussian fits to the experimental values we found the value of η in these experiments to be 40 ± 1 nm^{-1} s^{-1} and the value of κ to be 510 ± 50 s^{-1}. Furthermore, from the derivative of these fits (Figure 3b), we can extract the full width at half maximum (fwhm) of the curves, which quantifies the duration of the particle's formation, and the maximum growth rate of the particle. We find the fwhm to be 0.7 ± 0.6 ms and the maximum growth rate to be 0.49 ± 0.05 nm/ms. While to the authors' knowledge values for η and κ have never been found experimentally, these values of duration and reaction rate are much smaller than the time scales on the order of minutes and nanometers per minute, respectively, that have previously been reported for chemical synthesis.[28,29] We postulate that the different kinetics is due to the driving force of the applied voltage, which pushes reagents together faster than random diffusion.

During these experiments, a time delay, t_d, of up to ~130 s is observed between changing the voltage polarity and recording particle formation, shown as dashed lines in Figure 2b. This delay likely results from the stochastic nature of particle nucleation and formation at the surface of the pore, as observed in other precipitation experiments.[12] It represents the average time for a particle to nucleate large enough to stick in the pore. However, during this time, additional gold may form around the pore due to reagents and smaller gold particles that have time to traverse the pore before it fills. The reduction of this

dx.doi.org/10.1021/nl303576q | Nano Lett. XXXX, XXX, XXX−XXX

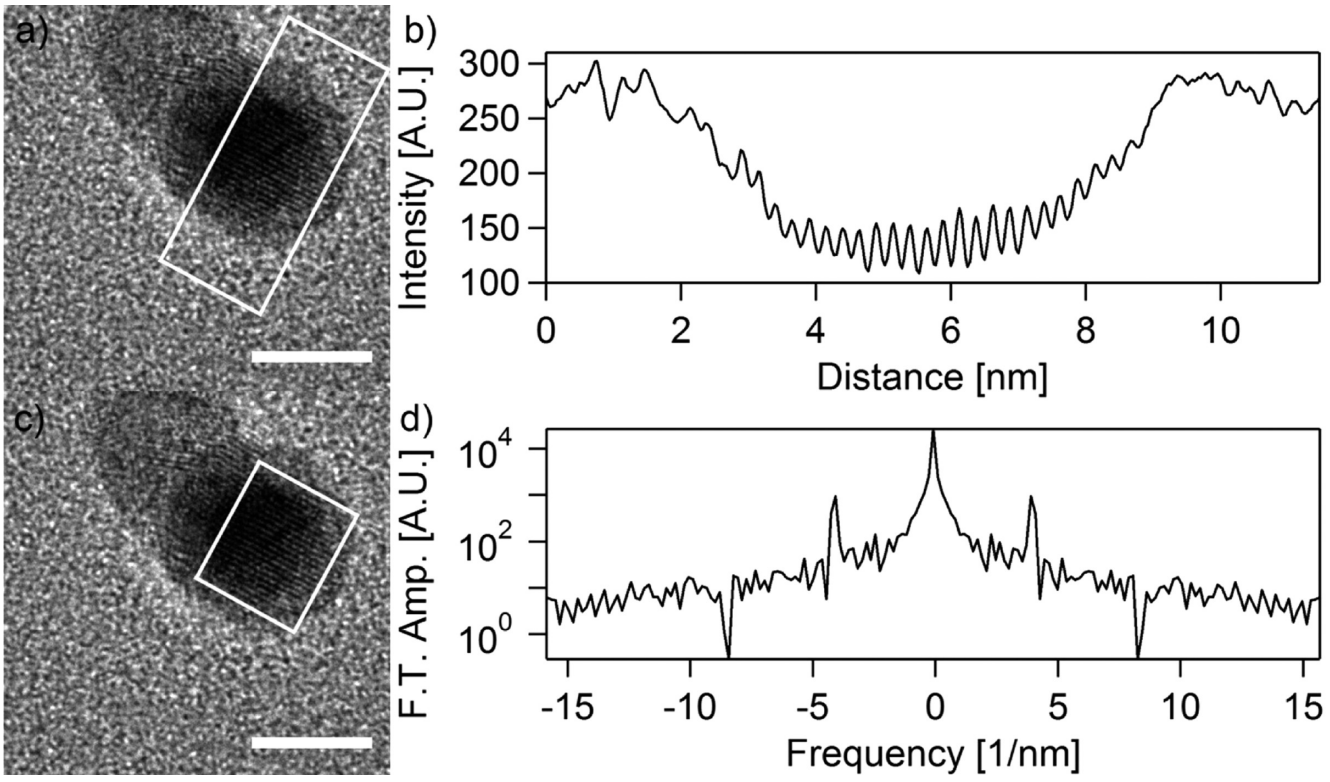

Figure 7. Determination of lattice spacing. (a) TEM image of a gold nanoparticle. The area inside the white box is used to create the (b) profile. The particle is crystalline and shows lattice planes within the crystal, whereas the SiN_x membrane surrounding the particle does not show lattice planes. The intensity profile data averaged over the depth of the white box in (c) is Fourier transformed to create (d). The peak value in panel d is at 3.95 nm^{-1}. The scale bar is 5 nm in panels a and c.

delay is thus crucial for eliminating additional particle formation at undesired places and for the particle's confinement to the pore volume.

We found that a reduction in the ionic strength of the electrolyte solution can be used to effectively reduce t_d. To quantify this effect, we recorded t_d for each experiment in KCl concentrations of 5 mM, 50 mM, and 1 M. Figure 4 shows t_d histograms for each KCl concentration from these experiments. 87.5% of t_d values were below 40 s, the maximum time displayed in Figure 4, for 1 M KCl, 83.9% were below 40 s for 50 mM KCl, and all values were below 40 s for 5 mM KCl. By decreasing the concentration of KCl in solution from 1 M to 50 mM or 5 mM, we found that t_d decreased by 1−2 orders of magnitude: for 1 M, $t_d = 15 \pm 1$ s; for 50 mM $t_d = 2.3 \pm 0.5$ s; and for 5 mM $t_d = 0.8 \pm 0.2$ s. These t_d values were extracted from Poisson fits. Decreasing the salt concentration increases the probability that any two oppositely charged ions interacting in the pore are reagents, thus increasing the reaction rate. We also studied the effect of pore diameter on t_d but found no observable trend (see Figure S4 in the Supporting Information).

Finally, we explored the effect of surface-capping additives on nanoparticle synthesis in a nanopore. We found that adding an organic molecule that binds to gold helps limit particle growth outside the pore. This method is used extensively for controlling the growth of nanoparticles in solution,[20] and we find its application extends well to particle growth inside nanopores. We used the additive α-lipoic acid as described above, which contains a disulfide group that binds to the gold surface with high affinity. It therefore caps the grown particle to prevent further aggregation of gold to the particle's surface.

Figure 5a shows a time trace of nanoparticle formation in the presence of α-lipoic acid. In experiments with this complex, when the polarity of the voltage is switched (Figure 5a (3)), the current shows only a capacitive curve that immediately decays to zero. That is, a particle forms very quickly (under 2 ms), and we cannot measure t_d. This is demonstrated in Figure 5b, which is the zoom-in of Figure 5a, and suggests that the particle completely forms faster than we can resolve with our setup. We performed $I-V$ traces before and after particle formation and verified that the particle fills the pore.

To illustrate the effects of salt concentration and additives, Figure 6 shows TEM images of particles formed at high salt concentration (1 M), at low salt concentration (50 mM), and at low salt concentration (50 mM) with α-lipoic acid. At low salt concentrations with or without α-lipoic acid, the nanoparticle is tightly confined in the nanopore area and there are no additional aggregates formed. See Figures S5 and S6 (Supporting Information) for examples of high salt aggregates. High-resolution TEM imaging shows that the particles are crystalline (Figure 7). From Fourier analysis of intensity line scans in the boxed areas in Figure 7c, we determined the lattice spacing to be 0.25 ± 0.05 nm as shown in Figure 7d, where the error is in our TEM's magnification, close to the published value of the 200 lattice spacing of 0.204 nm, as determined by X-ray crystallography.[30]

Nanoparticles formed using low salt concentrations and the α-lipoic acid gold chloride complex were restricted to the nanopore volume and showed no signs of additional particle formation over the entire silicon nitride membrane (Figure 6c). Based on TEM imaging, particles appear to conform to the shape of the pore (see Figure S7 in the Supporting Information

dx.doi.org/10.1021/nl303576q | Nano Lett. XXXX, XXX, XXX−XXX

for TEM images of a pore before and after particle formation). Further studies involving electron tomography could investigate the effect of pore shape[31] on the shape of the resulting particles. We also find that synthesized particles remained fixed inside of the pores. Even 18 days after formation, particles were observed fixed inside their pores in the TEM.

In conclusion, we demonstrate an original synthesis of nanoparticles with controllable size formed at a predetermined position in a thin solid-state membrane using electric field-driven electrolyte flow. Particle formation is electrically triggered and actively monitored by current readout, and the particle growth in time is quantitatively described by the Richards curve. Particle size and position is largely determined by the properties of a corresponding nanopore drilled at a desired position on a chip. Lowering salt concentration in solution and adding a capping agent improves particle confinement within the nanopore. Nanoparticles form orders of magnitude faster with this method than has been previously reported, and we can monitor their formation at time scales down to tens of microseconds. Future expansions of this work can focus on creating unique nanoparticle arrays with nanopores that are independently addressed by electric fields and expanding this method to other metals and materials. Finally, because each synthesized particle can be easily located, high-resolution TEM studies of the structure and shape of individual nanoparticles as a function of synthesis conditions are now possible.

■ ASSOCIATED CONTENT

Supporting Information

Optimal reagent ratio determination, control current traces, schematic and equivalent circuit of our nanopore, analysis of t_d with respect to pore size, TEM of gold formed in 1 M KCl, gold formation experiment in chips with multiple nanopores, and pore profiles before and after gold formation demonstrating particle containment inside the pore. This material is available free of charge via the Internet at http://pubs.acs.org.

■ AUTHOR INFORMATION

Corresponding Author

*E-mail: drndic@physics.upenn.edu.

Present Address

[†]Department of Physics, Northeastern University, Boston, Massachusetts 02115, United States.

Notes

The authors declare no competing financial interest.

■ ACKNOWLEDGMENTS

The authors thank Dr. Gabriel Shemer and Austin Joyce for useful discussions and Dr. Vishva Ray for marker fabrication. This material is based upon work supported by the National Science Foundation Graduate Research Fellowship (K.V.) under Grant No. DGE-0822. Any opinion, findings, and conclusions or recommendations expressed in this material are those of the authors and do not necessarily reflect the views of the National Science Foundation. K.V. acknowledges funding from the NSF-IGERT program (grant DGE-0221664). This work was supported in part by the MRSEC NSF grants DMR-0520020 and DMR-1120901 and NIH grant R21HG004767. We gratefully acknowledge use of the TEM in the NSF-MRSEC electron microscopy facility.

■ REFERENCES

(1) Sun, S. H.; Murray, C. B.; Weller, D.; Folks, L.; Moser, A. *Science* **2000**, *287*, 1989.
(2) Murray, C. B.; Kagan, C. R.; Bawendi, M. G. *Annu. Rev. Mater. Sci.* **2000**, *30*, 545.
(3) Bellapadrona, G.; Tesler, A. B.; Grunstein, D.; Hossain, L. H.; Kikkeri, R.; Seeberger, P. H.; Vaskevich, A.; Rubinstein, I. *Anal. Chem.* **2012**, *84*, 232.
(4) Hulteen, J. C.; Vanduyne, R. P. *J. Vac. Sci. Technol., A* **1995**, *13*, 1553.
(5) Haynes, C. L.; McFarland, A. D.; Smith, M. T.; Hulteen, J. C.; Van Duyne, R. P. *J. Phys. Chem. B* **2002**, *106*, 1898.
(6) Robbie, K.; Brett, M. J. *J. Vac. Sci. Technol., A* **1997**, *15*, 1460.
(7) Craighead, H. G.; Niklasson, G. A. *Appl. Phys. Lett.* **1984**, *44*, 1134.
(8) Gotschy, W.; Vonmetz, K.; Leitner, A.; Aussenegg, F. R. *Appl. Phys. B* **1996**, *63*, 381.
(9) Guo, P.; Martin, C. R.; Zhao, Y. P.; Ge, J.; Zare, R. N. *Nano Lett.* **2010**, *10*, 2202.
(10) Sharabani, R.; Reuveni, S.; Noy, G.; Shapira, E.; Sadeh, S.; Selzer, Y. *Nano Lett.* **2008**, *8*, 1169.
(11) Bouchet, A.; Descamps, E.; Mailley, P.; Livache, T.; Chatelain, F.; Haguet, V. *Small* **2009**, *5*, 2297.
(12) Innes, L.; Powell, M. R.; Vlassiouk, I.; Martens, C.; Siwy, Z. S. *J. Phys. Chem. C* **2010**, *114*, 8126.
(13) Wolfram, M. T.; Burger, M.; Siwy, Z. S. *J. Phys.: Condens. Matter* **2010**, *22*, 450301.
(14) Healy, K.; Schiedt, B.; Morrison, A. P. *Nanomedicine (U.K.)* **2007**, *2*, 875.
(15) Venkatesan, B. M.; Bashir, R. *Nat. Nanotechnol.* **2011**, *6*, 615.
(16) Wanunu, M. *Phys. Life Rev.* **2012**, *9*, 125.
(17) Storm, A. J.; Chen, J. H.; Ling, X. S.; Zandbergen, H. W.; Dekker, C. *Nat. Mater.* **2003**, *2*, 537.
(18) Fischbein, M. D.; Drndic, M. *Nano Lett.* **2007**, *7*, 1329.
(19) Murray, C. B.; Norris, D. J.; Bawendi, M. G. *J. Am. Chem. Soc.* **1993**, *115*, 8706.
(20) Brust, M.; Walker, M.; Bethell, D.; Schiffrin, D. J.; Whyman, R. *J. Chem. Soc., Chem. Commun.* **1994**, 801.
(21) Healy, K.; Ray, V.; Willis, L. J.; Peterman, N.; Bartel, J.; Drndić, M. *Electrophoresis* **2012**, *33*, 3488.
(22) Fischbein, M. D.; Drndic, M. *Appl. Phys. Lett.* **2006**, *88*, 063116.
(23) Wanunu, M.; Dadosh, T.; Ray, V.; Jin, J. M.; McReynolds, L.; Drndic, M. *Nat. Nanotechnol.* **2010**, *5*, 807.
(24) Bjerrum, J. *Stability constants of metal-ion complexes, with solubility products of inorganic substances*; Chemical Society: London, 1957.
(25) Smeets, R. M. M.; Keyser, U. F.; Krapf, D.; Wu, M. Y.; Dekker, N. H.; Dekker, C. *Nano Lett* **2006**, *6*, 89.
(26) Kasianowicz, J. J.; Brandin, E.; Branton, D.; Deamer, D. W. *Proc. Natl. Acad. Sci. U.S.A.* **1996**, *93*, 13770.
(27) Richards, F. J. *J. Exp. Botany* **1959**, *10*, 290.
(28) Liu, X.; Worden, J. G.; Huo, Q.; Brennan, J. R. *J. Nanosci. Nanotechnol.* **2006**, *6*, 1054.
(29) Polte, J.; Erler, R.; Thunemann, A. F.; Sokolov, S.; Ahner, T. T.; Rademann, K.; Emmerling, F.; Kraehnert, R. *ACS Nano* **2010**, *4*, 1076.
(30) Weast, R. C. *CRC Handbook of Chemistry and Physics*; 1st student ed.; CRC Press: Boca Raton, FL, 1988.
(31) Kim, M. J.; Wanunu, M.; Bell, D. C.; Meller, A. *Adv. Mater.* **2006**, *18*, 3149.